A98-31481

ICAS-98-1,10,2

Closed-Loop Constrained Control Allocation for a Supermanoeuvrable Aircraft

B. Dang-Vu and D. Brocas
Office National d'Etudes et de Recherches Aérospatiales (ONERA)
BA 701 - 13661 Salon de Provence - France

Abstract

Recent research into the problem of allocating flight control effectors to generate specified moments has explored techniques that achieve the maximum attainable aircraft moment. The contribution of this paper is to incorporate open-loop control allocators obtained from such techniques inside a closed-loop dynamic inversion control law. The combined approach is used to design the flight control law of a supermanoeuvrable aircraft.

The simulation results of a velocity roll manoeuvre are compared with two other most commonly used control allocation techniques : pseudo-inverse and daisy-chaining. When the controls reach saturation, it is shown that the use of moderate sideslip can significantly increase the attainable moment subset at high angle of attack flight regime.

A μ-analysis is conducted to assess the stability robustness of the control law to modelling uncertainties.

Nomenclature

V	Airspeed
α, β	Angle of attack and sideslip
p, q, r	Body-axis roll, pitch and yaw rates
p_w	Wind-axis roll rate
μ	Velocity bank angle
	Structured singular value
γ	Flight path angle
n_{y_a}, n_{z_a}	Lateral and normal load factors
δ_e	Horizontal tail deflection
δ_a	Aileron deflection
δ_r	Rudder deflection
δ_{tv}	Thrust-vectoring
x	State vector
u	Control inputs vector
y	Controlled vector
Ω	Angular rotation rate vector
m	Moment vector
I_x, I_y, I_z	Moments of inertia
c	Reference length
S	Reference area
$\bar{q}$	Dynamic pressure
Subscript	
c, cmd	Commanded

Introduction

A significant work has been published using nonlinear dynamic inversion methods as an approach to design flight control laws for supermanoeuvrable aircraft. The methodology is based upon straightforward manipulations of the equations of flight mechanics from which state-dependent forces and moments for the control to generate can be specified. The last step in dynamic inversion is to solve for the control vector which is constrained to certain limits. This is referred to as constrained control allocation.

The pseudo-inverse has been a standard method for solving control allocation problems due to the ease with which it can be calculated. However, for arbitrary moment demands, that method cannot yield solutions that attain the maximum available moment without violating some control constraint.

Recent research into the problem of allocating flight control effectors to generate specified moments has explored techniques that achieve the maximum attainable aircraft moment[1-4]. For a supermanoeuvrable aircraft, it is indeed natural to find the proper combination of controls which produces the demanded moment for manoeuvring while maximizing the margin of control power available for stabilization.

The contribution of this paper is to incorporate control allocators obtained from such techniques inside a closed-loop dynamic inversion control law. This paper is organized as follows: The structure of the inverse dynamics controller is first introduced after a short review of the main features of the dynamic inversion techniques. The linearizing transformations which lead to the expression of the moments for the controls to generate are then developed. The section following describes the problem of control allocation in geometric terms and presents the so-called 'direct method' which solves for the controls. In the next section the simulation results of a velocity roll manoeuvre are compared with two other most commonly used control allocation techniques: pseudo-inverse and daisy-chaining.

The use of sideslip to extend the attainable moment subset is then investigated. Finally, as dynamic inversion control techniques are not inherently robust, a μ-analysis is conducted to assess the stability robustness of the control law to modelling uncertainties.

Non-linear Dynamic Inversion Control

Among the specific methodologies for the control of systems described by non-linear mathematical models, dynamic inversion is certainly the most widely investigated by control researchers in the last three decades. A complete theory is now available for the design of feedback control laws which render certain outputs independent of certain inputs (disturbance decoupling and non-interactive control) or which transform a non-linear system into an equivalent linear system (feedback linearization or dynamic inversion).

As the input-output behaviour of the resulting state-feedback resembles that of a linear time-invariant system, any linear control design technique can be applied to achieve the design performance.

There have been many applications of non-interacting control and feedback linearization to aircraft flight control problems[6-17]. The main advantage of this technique is that the use of a single equivalent linear system requires minimal gain scheduling effort to provide desired handling qualities over a wide range of flight conditions. Traditional aircraft control designs have to rely on many locally linearized models obtained throughout the flight envelope of the vehicle, with linear controllers synthesized for the set of resulting linearized models.

As shown on the block diagram of Fig. 1, the controller has been split into three main blocks: linear time-invariant dynamics resulting from feedback linearization, non-linear inverse dynamics which yield the moments for the controls to generate, and control allocation which distributes the effort between the available control effectors.

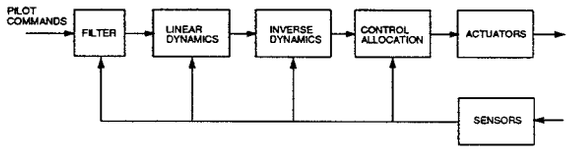

Figure 1: Non-linear inverse dynamics control system

After shaping and filtering, the pilot command vector is defined as

$$y_{cmd} = (q_{cmd}, p_{wcmd}, \beta_{cmd})^T$$

where q_{cmd} is the commanded body-axis pitch rate, p_{wcmd} is the commanded wind-axis roll rate, and β_{cmd} is the commanded sideslip angle.

Pitch rate commands required for the limitation of angle of attack $q_{\alpha lim}$ and normal acceleration q_{nlim} are also generated. The pilot pitch command is therefore saturated following

$$q_c = min(q_{cmd}, q_{\alpha lim}, q_{nlim})$$

Assuming that there is sufficient time-scale separation between the translational and rotational variables, the calculations of the linearizing transformations can be simplified by using singular perturbation theory[10]. The body-axis angular rates commands p_c, q_c , and r_c are thus used as control inputs to the system driving the sideslip and the angle of attack. Indeed, as $\dot{\alpha}$ and $\dot{\beta}$ are affine in p, q, and r, a non-linear inverse can be easily defined. The commanded body-axis roll and yaw rates can be solved from the following algebraic equations

$$\begin{aligned} p_{wcmd} &= \frac{1}{\cos\beta}(p_c\cos\alpha + r_c\sin\alpha) \\ &\quad -\frac{g}{V}(n_{z_a} + \cos\gamma\cos\mu)\tan\beta \\ \omega_\beta(\beta_{cmd} - \beta) &= p_c\sin\alpha - r_c\cos\alpha \\ &\quad +\frac{g}{V}(n_{y_a} + \cos\gamma\sin\mu) \end{aligned}$$

The required pitch rate for angle of attack limitation is given by

$$\begin{aligned} q_{\alpha lim} &= \omega_\alpha(\alpha_{max} - \alpha) + (p_c\cos\alpha + r_c\sin\alpha)\tan\beta \\ &\quad -\frac{g}{V\cos\beta}(n_{z_a} + \cos\gamma\cos\mu) \end{aligned}$$

The same expression is used to calculate the required pitch rate for normal acceleration limitation, the maximum angle of attack α_{max} being in that case a function of the dynamic pressure. The frequencies ω_β and ω_α will be scheduled such to fulfill the handling qualities requirements over the entire flight envelope.

It should be noted that the use of the acceleration components n_{y_a} and n_{z_a} in the expressions of the commanded angular rates prevent from neglecting the control effects in the equations of forces as usually done.The angular rotation accelerations given by the equations of moments

$$\dot{\Omega} = \begin{bmatrix} \dot{p} \\ \dot{q} \\ \dot{r} \end{bmatrix} = f(x,u)$$

are now shaped to the following desired dynamics

$$f_d = \begin{bmatrix} \omega_p(p_c - p) + \omega_{p\beta}(\beta - \beta_{cmd}) \\ \omega_q(q_c - q) \\ \omega_r(r_c - r) \end{bmatrix}$$

These dynamics are the actual closed-loop input/output relation after applying feedback linearization to the set of equations of moment. It is important to note that the desired dynamics contain a coupling term between the lateral and the directional axes corresponding to the dihedral effect. A strict decoupling would lead to excessive control activities. The frequencies $\omega_p, \omega_q, \omega_r$, and $\omega_{p\beta}$ will be scheduled such to fulfill the handling qualities requirements over the whole flight envelope.

To solve for the control vector u such that

$$f(x,u) = f_d$$

at any operating point, we consider only the moments to generate by the controls, after eliminating all the

other aerodynamic and inertial moments. Thus we define the commanded moments generated as pseudo-control variables

$$m_d = f_d - f(x, u_0)$$

where u_0 is filtered from the instantaneous control, i.e

$$\frac{u_0(s)}{u(s)} = \frac{1}{1+\tau s}$$

The next section addresses the problem of the allocation of the controls to the generation of the above specified body-axis moments. The control inputs to the vehicle, a model of a supermanoeuvrable fighter aircraft, include the horizontal tail δ_e, the differential aileron δ_a, the rudder δ_r and the pitch thrust-vectoring δ_{tv}. The allocation of effort between these control surfaces can be accomplished by a variety of methods.

Control allocation

This step in dynamic inversion is to solve for the control vector which is constrained to certain limits

$$u_{imin} \leq u_i \leq u_{imax} \quad i = 1, ..., l$$

Amplitude limiting of actuators are non-linearities that cannot be treated by most non-linear control design techniques, e.g. dynamic inversion. Methods based on time-optimal control do not saturate but remain difficult to be incorporated in flight systems. Progress has been made in designing systems that consider these saturations. The concept of tracking a less aggressive reference as a means of avoiding saturation has been proposed. It consists of designing a control loop that modifies the error signal (difference between the pilot command and the actual response) so that saturation does not occur[18]. Another approach is based on a gain scheduling by Lyapunov functions[19].

As the dynamic inversion technique used herein specifies instantaneous moments for the controls to generate, it is natural to find the proper combination of controls which produces the demanded moment while maximizing the margin of control power available for stabilization. Recent research into the problem of allocating flight control effectors to generate specified moments has indeed explored techniques that achieve the maximum attainable aircraft moment[1-4]. The contribution of our work is to incorporate open-loop non-linear control allocators obtained from such techniques inside the closed-loop dynamic inversion control law developed above.

The so-called 'direct method' consists of two parts: the determination of the attainable moment subset

$$\Phi = (m | u_{imin} \leq u_i \leq u_{imax} \quad i = 1, ..., l)$$

where

$$m = f(x, u) - f(x, u_0)$$

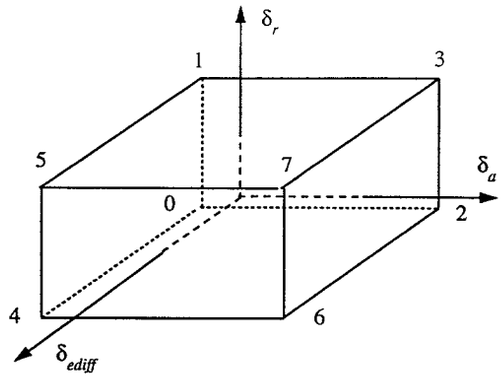

Figure 2: Admissible controls

and the calculation of the controls that yield moments within and on the boundary $\partial(\Phi)$ of that subset without violating the control constraints. Then, given some desired moment m_d

$$m_d = f_d - f(x, u_0)$$

the problem becomes finding the controls u that generate that moment for the largest possible magnitude of m in the direction m_d. A geometric approach is introduced which consists of the identification of the point of intersection of the line in the direction of the desired moment m_d with the boundary of the attainable moment subset, the calculation of the controls that generate that intersection, and finally scaling of the controls in proportion with the desired moment.

Two-Moment Problem

For the purpose of illustration of the method, let us consider the three constrained controllers

$$u = (\delta_{ediff}, \delta_a, \delta_r)^T$$

differential horizontal tail, differential aileron, and rudder (Fig. 2). Associated with these controllers we consider the two-dimensional space whose coordinates are the third and second components of m. The moments are normalized with respect to $\bar{q}ScI_z$ and $\bar{q}ScI_x$ respectively and are denoted C_n and C_l (Fig. 3).

The points corresponding to the limit values of the controls are called vertices, and numbered according to a binary representation, a '0' in the ith significant figure of the binary number indicates that the ith control is a minimum, and a '1' indicates a maximum. For example, the vertex corresponding to $\delta_{ediff} = +20$ deg, $\delta_a = -20$ deg and $\delta_r = -20$ deg is binary 100, or decimal 4 as illustrated in Fig. 2.

The moments produced by constrained controls may be expressed as a mapping of the subset of constrained controls into the moment space. This results in a closed subset of attainable moments.

In Fig. 3, each point of the figure represents the moment generated by a combination of three controls

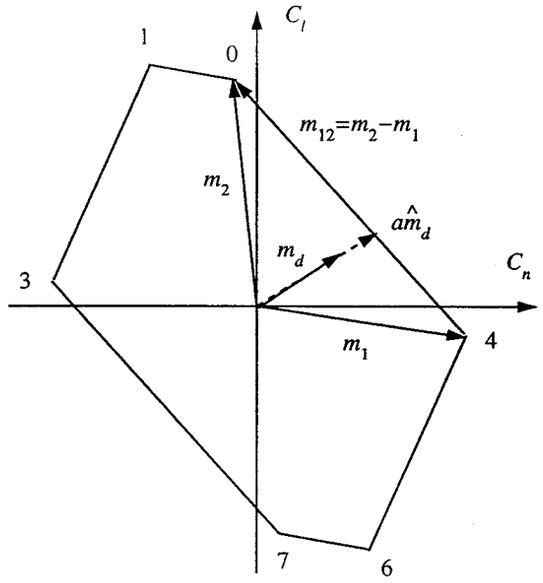

Figure 3: Geometric inversion

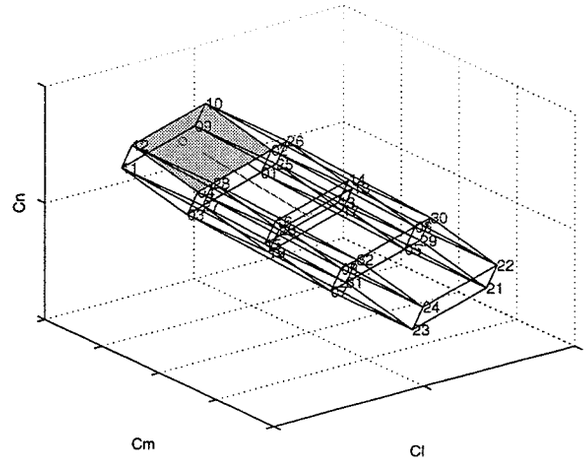

Figure 4: Boundary of the attainable moment subset

at one or the other of their constraints. The boundary $\partial(\Phi)$ of the attainable moment subset is represented by the convex polygon 0-1-3-7-6-4. All the other points are inside the boundary and not represented. When the number of controls is greater than the dimension of the moment space, there are infinite combinations of admissible controls that generate moments in the interior of the attainable moment subset, but on the boundary the combinations are unique. Based on this result, the direct method calculates admissible controls in the interior of the attainable moment subset as scaled-down versions of the unique solutions on the boundary and provides continuous solutions for continuously varying moment demands.

The desired moment is expressed under the normalized form

$$m_d = |m_d|\hat{m}_d$$

where

$$|\hat{m}_d| = 1$$

Let m_1 and m_2 the two moment vectors of the boundary $\partial(\Phi)$ which define the edge $m_{12} = m_2 - m_1$ to which the desired moment vector m_d is pointed. At the intersection of the half-line in the direction of m_d and the facet m_{12}, we have

$$a\hat{m}_d = m_1 + bm_{12}$$

with $a > 0$ and $0 \leq b \leq 1$. At this point the control is given by

$$u^* = u_1 + b(u_2 - u_1)$$

where u_1 and u_2 are the controls associated with m_1 and m_2 respectively. Defining the components for the moment vectors

$$m_d = \begin{bmatrix} m_d^1 \\ m_d^2 \end{bmatrix} \quad m_1 = \begin{bmatrix} m_1^1 \\ m_1^2 \end{bmatrix} \quad m_{12} = \begin{bmatrix} m_{12}^1 \\ m_{12}^2 \end{bmatrix}$$

yields

$$\begin{bmatrix} a \\ b \end{bmatrix} = \begin{bmatrix} m_d^1 & -m_{12}^1 \\ m_d^2 & m_{12}^2 \end{bmatrix}^{-1} \begin{bmatrix} m_1^1 \\ m_1^2 \end{bmatrix}$$

The desired combination of controls is finally

$$u = ku^*$$

with

$$k = \frac{|m_d|}{a}$$

Three-Moment Problem

The solution to the three-moment problem is less trivial. The difficulties concern the determination of the boundary of the attainable moment subset, and the identification of the applicable part of the bounding surface, that is the facet where the desired moment points to. The method for determining these surfaces is taken from Reference 2.

Once the applicable part of the bounding surface is identified, the determination of the controls that generate a desired moment on the surface of the attainable moment subset is easy. Assume that the facet is defined by the vertex m_i and the edges m_{ij} and m_{ik}, the intersection with the desired moment m_d is calculated from the equation

$$a\hat{m}_d = m_i + bm_{ij} + cm_{ik}$$

where $\hat{m}_d$ is the unit vector in the direction of m_d and

$$a > 0 \quad 0 \leq b \leq 1 \quad 0 \leq c \leq 1$$

This yields

$$\begin{bmatrix} 1/a \\ b/a \\ c/a \end{bmatrix} = \begin{bmatrix} m_i & m_{ij} & m_{ik} \end{bmatrix}^{-1} \hat{m}_d$$

At the intersection, the control is then

$$u^* = u_i + bu_{ij} + cu_{ik}$$

where u_i, u_{ij}, and u_{ik} are associated with m_i, m_{ij} and m_{ik} respectively. The desired combination of controls is finally

$$u = ku^*$$

with

$$k = \frac{|m_d|}{a}$$

Fig. 4 and Fig. 5 show the results of a five-control, three-moment problem. The flight condition at which the moment subset is determined is 100 KCAS, altitude 30,000 ft and 50 deg angle of attack.

The control inputs vector is

$$u = (\delta_{tv}, \delta_{eright}, \delta_{eleft}, \delta_a, \delta_r)^T$$

with the following limits: thrust vectoring $\delta_{tv} = \pm 20$ deg, right horizontal tail $\delta_{eright} = \pm 40$ deg, left horizontal tail $\delta_{eleft} = \pm 40$ deg, aileron $\delta_a = \pm 30$ deg, and rudder $\delta_r = \pm 30$ deg. For all controls, the effectiveness varies non-linearly with the deflection. Interference from different control deflections results also in changes in effectiveness. By considering the combinations of the controls only at one or the other of their constraints, the mapping of the subset of controls into the moment space leads to a polytopic approximation of the boundary $\partial(\Phi)$.

In Fig. 4, the desired moment is within the boundary. To aid in visualisation, the facet the desired moment vector points to has been greyed. We find the controls that generate the point of intersection and we scale down the controls with the factor k. The result is

$$u = (-16.78; 13.82; -33.55; 3.55; 33.55)^T \ (units : deg)$$

In Fig. 5, the desired moment is outside the boundary, then no combination of controls can generate it, and we take the controls that generate the intersection as being the best that can be done

$$u = (20; 3.47; -14.52; 30; -40)^T$$

The thrust vectoring is at its maximum +20 deg, the aileron at its maximum +30 deg and the rudder at its minimum -40 deg.

Simulation results

The simulation includes the six degree-of-freedom non-linear dynamics of the aircraft, limits on control surface deflections and rates, and aerodynamic coefficient obtained from look-up tables as functions of angle of attack.

The application consists of an on-line calculation of the feedback linearizing transformations including bandwith scheduling, on-line determination of the attainable moment subset at any flight operating point, and on-line control allocation using the direct method.

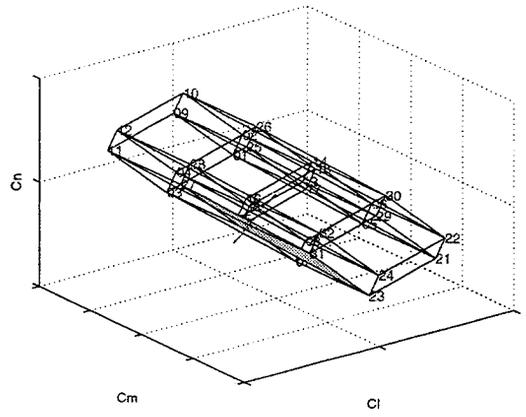

Figure 5: Boundary of the attainable moment subset

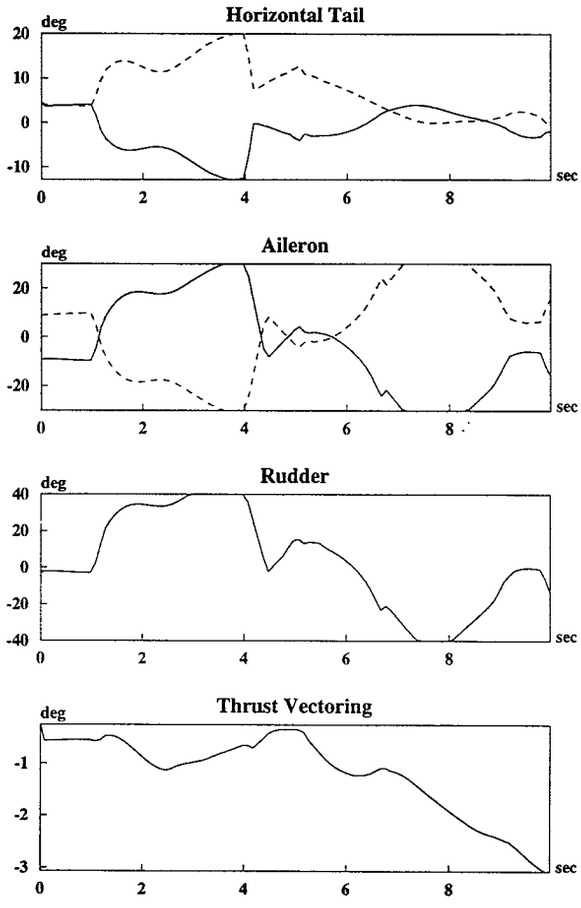

Figure 6: Control time histories

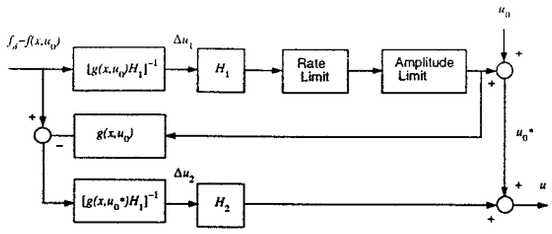

Figure 7: Daisy-chaining allocation

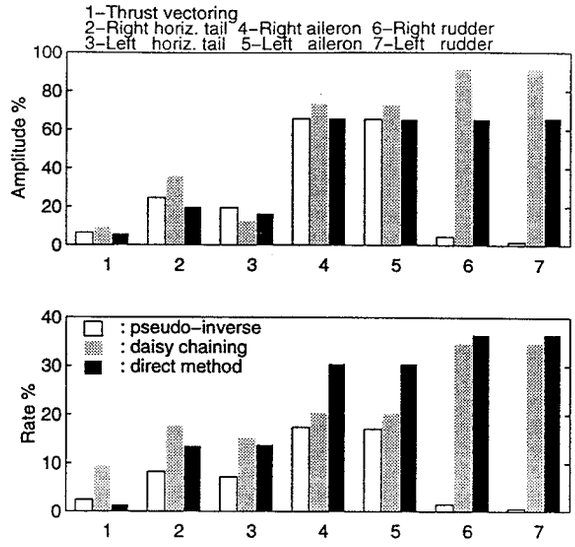

Figure 8: Control activities

The control law was tested for a roll manoeuvre about the velocity vector at low dynamic pressure (100 KCAS, altitude 30,000 ft) and 50 deg angle of attack.

The time histories of the control deflections are plotted in Fig. 6. The left horizontail tail and the left aileron are plotted in dashed lines. The step command in roll rate was chosen such to put the control surfaces to saturation. It is seen indeed that between $t = 3$ and 4 sec, the demand exceeds the capabilities of the controls. The contribution of the different control surfaces deserves some explanation. The rudder saturates during the roll because at 50 deg angle of attack, its effectiveness is considerably reduced. The yawing moment required to coordinate the velocity roll is then generated by a differential deflection of the horizontal tail. This produces however an opposite rolling moment, and therefore an additional deflection of aileron is necessary. The maximum roll rate is then obtained at the saturation of the aileron. Thrust-vectoring in pitch is little used because the horizontal tail is still effective.

Two other methods of control allocation were also simulated for comparison: pseudo-inverse and daisy-chaining.

The pseudo-inverse has been a standard method for solving control allocation problems due to the mathematical ease with which it can be calculated. The solution minimizes the Euclidean norm of the control vector. After linearizing the equations of moments

$$f(x,u) = f(x,u_0) + g(x,u_0)(u - u_0)$$

where $g(x,u_0)$ is the linearized control effectiveness matrix, we solve for the desired moment

$$f(x,u) = f_d$$

to obtain the control

$$u = u_0 + T[g(x,u_0)T]^{\sharp}[f_d - f(x,u_0)]$$

where $^{\sharp}$ denotes the pseudo-inverse.

We scale the control deflections by means of a weighting matrix T according to their relative effectiveness and according to the flight conditions. For arbitrary moment demands, the pseudo-inverse method cannot yield solutions that attain the maximum available moment without violating some control constraint[4]. An optimization procedure can be performed by adjusting the elements of the weighting matrix until a desired performance is reached.

At high angle of attack, the effectiveness of the rudder is reduced and the pseudo-inverse yields a minimum deflection solution, which is opposite to the one provided by the direct allocation method (Fig. 8).

The daisy-chaining method involves the separation of the available controls in two or more groups. As any of the controls in the group being applied reaches saturation, that group is held in its last position and another group is brought on line to continue generating the required moments. For the present application, two groups of control are selected. The first one u_1 includes three aerodynamic controls: symmetric horizontal tail δ_{esym}, differential aileron δ_a and rudder δ_r. The second one u_2 includes pitch thrust-vectoring δ_{tv}, differential aileron δ_a and differential horizontal tail δ_{ediff}. At high angle of attack, the pitching control moment is supplied by the thrust-vectoring, and the yawing control moment is supplied by the differential horizontal tail. The block diagram of the daisy-chaining allocation is shown in Fig. 7. To solve for

$$f(x,u) = f_d$$

the equations of moments are linearized with respect to the controls

$$f(x,u) = f(x,u_0) + g(x,u_0)(u - u_0)$$

For a given moment to be generated, the aerodynamic controls are first used to the point where one or more controls are saturated

$$\begin{aligned} u - u_0 &= H_1 \Delta u_1 \\ \Delta u_1 &= [g(x,u_0)H_1]^{-1}[f_d - f(x,u_0)] \end{aligned}$$

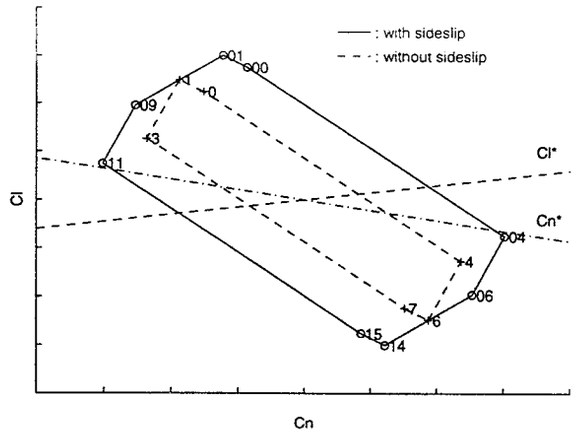

Figure 9: Extended attainable moment subset

Then the second group is brought to bear

$$\begin{aligned} u_0^* &= u_0 + H_1 \Delta u_1 \\ u - u_0^* &= H_2 \Delta u_2 \end{aligned}$$

and

$$\Delta u_2 = [g(x, u_0^*) H_2]^{-1} [f_d - f(x, u_0) - g(x, u_0) H_1 \Delta u_1]$$

, When none of the aerodynamic controls of the first group are saturated, we have $\Delta u_2 = 0$.

From Fig. 8, it is seen that both the direct method and the daisy-chaining method have the highest control activities.

Daisy chaining cannot access all the attainable moments while the direct method can[4]. To reduce the control actuator rates demand, one solution consists of applying the direct method to moment-rate allocation[5]. But there is a flexibility in choosing the rate demand characteristics only within the strict interior of the attainable moment subset.

Extension of the attainable moment subset To achieve high performance it is necessary to use all the available control power, but saturation can lead to instability. It is then required that the control does not remain in saturation if saturation occurs. For the velocity roll manoeuvre at high angle of attack, this can achieved by applying a sideslip command order. The attainable moment subset plotted in Fig. 9 shows that the use of sideslip provides an extended region of controllability in roll and yaw[20]. The dashed line boundary represents the case where there is no sideslip. The solid line boundary corresponds to a ± 5 deg of sideslip.

The vertices corresponding to the limit values of the controls are numbered according to a binary representation, a '0' in the ith significant figure of the binary number indicates that the ith control is a minimum, and a '1' indicates a maximum. The controls are arranged as follows

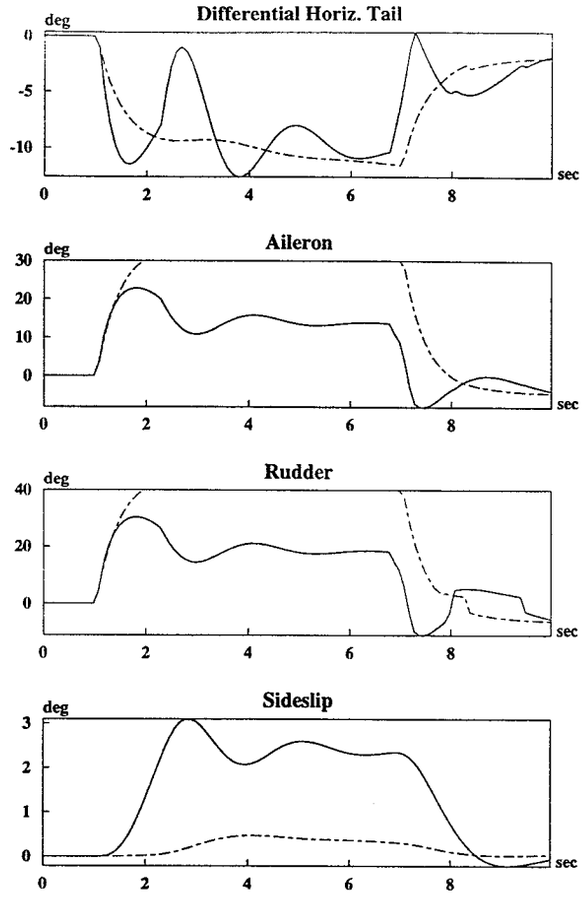

Figure 10: Control desaturation

$(\delta_{ediff}, \delta_a, \delta_r)$ when $\beta = 0$, and
$(\beta_{cmd}, \delta_{ediff}, \delta_a, \delta_r)$ when $\beta \neq 0$.

We also plot in Fig. 9 the stability-axis moment coefficients

$$\begin{aligned} C_n^* &= C_n \cos\alpha - \frac{I_z}{I_x} C_l \sin\alpha \\ C_l^* &= (C_l \cos\alpha + \frac{I_x}{I_z} C_n \sin\alpha) \frac{1}{\cos\beta} \end{aligned}$$

which are representative of a yaw acceleration and a roll acceleration about the velocity vector that can be generated by the controls. The intersection of the C_n^* axis (mixed line) with the attainable moment subset boundary determines the capability of sideslip control without induced roll. The intersection of the C_l^* axis (dashed line) with the attainable moment subset boundary determines the capability of velocity roll control without induced sideslip. We now illustrate the above analysis by means of a simulation of a velocity roll manoeuvre (Fig. 10). The step command in roll rate was chosen such to put the control surfaces to saturation (mixed lines). The left horizontal tail and the left aileron are not plotted in the figure. It should be noted that the transient sideslip is very small during the roll.

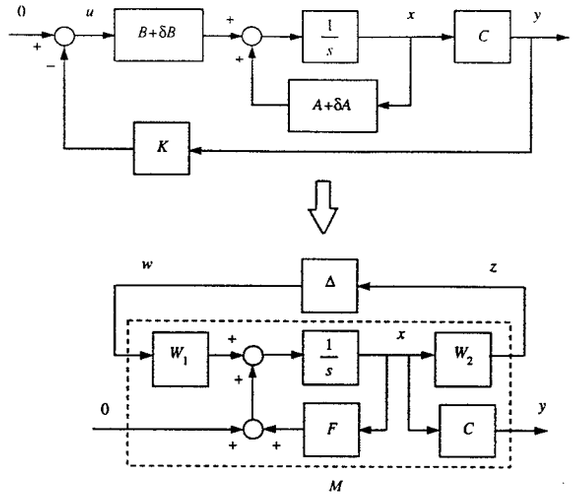

Figure 11: LFT of the pametric perturbated model

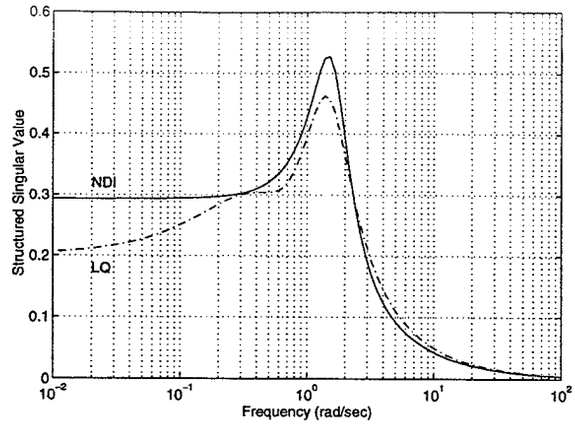

Figure 12: SSV. Lateral controller

Now, by applying the direct allocation method to the attainable moment subset generated by the four controls $(\beta_{cmd}, \delta_{ediff}, \delta_a, \delta_r)$, a commanded sideslip is calculated on-line. The control time histories (solid lines) show clearly that the controls do not remain in saturation.

Robustness Analysis

Dynamic inversion control techniques are not inherently robust. A stability robustness analysis is then conducted to check the tolerance of the controller to model uncertainties.

A linearized model of the aircraft (A, B, C) with its controller K is used to assess the robustness of the controller. Linear Fractional Transformations (LFT's) provide a general concept to include uncertainties on transfer matrices or state space realizations[21]. To derive an LFT representation, the invariant part of the model and the uncertain part are separated. Most of the existing work on robust analysis view model uncertainties as fractional variations of the design-model parameters. Each of the unknown elements of the matrices $A+\delta A$ and $B+\delta B$ are thus expressed under the form

$$\begin{aligned} a_{ij} &= a^0_{ij}(1+\alpha_{ij}\delta^a_{ij}) \quad i=1,...n \quad j=1,...,n \\ b_{ik} &= b^0_{ik}(1+\beta_{ik}\delta^b_{ik}) \quad i=1,...n \quad k=1,...,l \end{aligned}$$

where the elements a^0_{ij} and b^0_{ik} of the matrices A and B are nominal values assumed to be constant, α_{ij} and β_{ik} are nominal dispersions, and δ^a_{ij}, $|\delta^a_{ij}| < 1$ and δ^b_{ik}, $|\delta^b_{ik}| < 1$ represent normalized uncertainties and are diagonally augmented in the perturbation matrix $\Delta = diag(...\delta^a_{ij}...\delta^b_{ik}...)$.

Fig. 11 shows the LFT representation of the closed-loop plant.

z and w are the inputs and outputs of the uncertainty block Δ, and W_1 and W_2 are weighting matrices. The LFT structure can be created using Morton's method[22]. For the present application, we write the closed-loop state space model as:

$$\begin{aligned} \dot{x} &= (A-BKC)x + (\delta A - \delta BKC)x \equiv Fx + W_1 w \\ y &= Cx \end{aligned}$$

As

$$w = \Delta z$$

and

$$z = W_2 x$$

the weighting matrices W_1 and W_2 can be obtained from

$$W_1 \Delta W_2 = \delta A - \delta BKC$$

Then the matrix that represents the system interconnection structure is given by

$$M(s) = W_2(sI - F)^{-1}W_1$$

The structured singular value of the complex matrix M with respect to the set of uncertainty matrices Δ is

$$\mu(M) = [inf(k \in [0,\infty]/\exists\Delta : det(I - k\Delta M) = 0)]^{-1}$$

The fundamental result concerning robust stability analysis using μ is that the system remains stable for any Δ if and only if:

$$\forall\omega \in I\!R \quad \mu(M(j\omega)) < 1$$

$\mu(\omega)^{-1}$ represents the size of the smallest parameter perturbation which brings one closed-loop pole on the imaginary axis at $\pm j\omega$. Robust stability is therefore guaranteed for any δ_i such that $|\delta_i| < min(\mu(\omega)^{-1})$.

The μ-plot of the lateral controller is shown in Fig. 12. The linearized aircraft model is at 50 deg angle of attack. The nominal dispersions α_{ij} and β_{ik} vary

between 20 percent and 50 percent depending on the elements of A and B. The solid line represents the μ-plot of the dynamic inversion controller. Since the structured singular value is less than one at all frequencies, the stability robustness is met. Furthermore, as the maximal value is about 0.5, stability is guaranteed for uncertainties which are almost twice the nominal dispersions. For comparison purposes, the μ-plot of a LQ controller is represented by the mixed line in Fig. 12.

Stability robustness can be further improved by synthesizing a robust, outer-loop controller around the dynamic inversion inner loop. It is well known that integral control improves robustness to parameter uncertainties and helps to eliminate steady-state tracking errors. A common approach is to design the outer-loop using structured singular value techniques[13-14].

Conclusion

In this paper, we have introduced an approach to design flight control laws which combines a non-linear dynamic inversion method and a non-linear geometric inversion for control allocation. The controller incorporates the full non-linear inertial dynamics and aerodynamics into its design. The method of control allocation guarantees the maximum generated moments within the control constraints. The methodology requires little scheduling effort with flight conditions.

The control design has been applied to a model of a supermanoeuvrable aircraft. The simulations which have been performed show the good performance of the closed-loop control allocation technique.

A μ-analysis is used to check the stability robustness of the dynamic inversion controller. It proved the stability of the controller despite parameter uncertainties.

References

[1]Durham W.C., 'Constrained Control Allocation', *Journal of Guidance, Control, and Dynamics*, Vol. 16, No. 4, 1993, pp. 717-725.

[2]Durham W.C., 'Constrained Control Allocation : Three-Moment Problem', *Journal of Guidance, Control, and Dynamics*, Vol. 17, No. 2, 1994, pp. 330-336.

[3]Durham W.C., 'Attainable Moments for the Constrained Control Allocation Problem', *Journal of Guidance, Control, and Dynamics*, Vol. 17, No. 6, 1994, pp. 1371-1373.

[4]Durham W.C., 'Closed-Form Solutions to Constrained Control Allocation Problem', *Journal of Guidance, Control, and Dynamics*, Vol. 18, No. 5, 1995, pp. 1000-1007.

[5]Durham W.C. and Bordignon K.A., 'Multiple Control Effector Rate Limiting', *AIAA Guidance, Navigation, and Control Conference*, Baltimore, MA, AIAA-95-3208, 1995.

[6]Asseo S.J., 'Decoupling a Class of Nonlinear Systems and its Application to an Aircraft Control Problem', *Journal of Aircraft*, Vol. 10, 1973, pp. 739-747.

[7]Singh S.N. and Schy A., 'Output Feedback Nonlinear Decoupled Control Synthesis and Observer Design for Maneuvering Aircraft', *International Journal of Control*, Vol. 31., 1980, pp. 781-806.

[8]Meyer G. and Cicolani L., 'Application of Nonlinear System Inverses to Automatic Flight Control Designs System Concepts and Flight Evaluations', *Theory and Application of Optimal Control in Aerospace Systems*, AGARD AG251, 1981, pp. 10.1-10.29.

[9]Dang-Vu B. and Mercier O.L., 'A Nonlinear Flight Control Law for Air-to-Ground Gunnery', *Integration of Fire Control, Flight Control and Propulsion Control Systems*, AGARD CP349, 1983, pp. 21.1-21.10.

[10]Menon P.K.A., Badgett M.E. and Walker R.A., 'Nonlinear Flight Test Trajectory Controllers for Aircraft', *AIAA Guidance and Control Conference*, Snow Mass, CO, AIAA-85-1890, 1985.

[11]Lane S.H. and Stengel R.F., 'Flight Control Design Using Nonlinear Inverse Dynamics', *Automatica*, Vol. 24, No. 4, 1988, pp. 471-483.

[12]Bugajski D.J., Enns D.F. and Elgersma M.R., 'A Dynamic Inversion Based Control Law with Application to the HARV', *AIAA Guidance, Navigation, and Control Conference*, Portland, OR, AIAA-90-3407, 1990.

[13]Adams R.C., Buffington J.M., Sparks A.G. and Banda S.S., 'Robust Multivariable Flight Control', *Advances in Industrial Control*, Springer-Verlag, Berlin, 1994.

[14]Reiner J., Balas G.J., and Garrard W.L., 'Robust Dynamic Inversion for Control of Highly Maneuverable Aircraft', *Journal of Guidance, Control, and Dynamics*, Vol. 18, 1995, pp. 18-24.

[15]Dang-Vu B., 'Design of Forebody Strakes and Thrust Vectoring Control Laws for Enhanced Maneuvering', *Proceedings of the Workshop on Full Envelope Agility*, Eglin AFB, Florida, 1995.

[16]Dang-Vu B., 'Nonlinear Dynamic Inversion Control', *Lectures Notes in Control and Information Sciences*, Vol. 224. Robust Control - A Design Challenge, Springer, 1995, pp. 102-111.

[17]Escande B., 'HIRM Design Challenge - Nonlinear Dynamic Inversion and LQ Techniques', *Lectures Notes in Control and Information Sciences*, Vol. 224. Robust Control - A Design Challenge, Springer, 1995, pp. 102-111.

[18]Kapasouris P., Athans M., and Stein G., 'Design of Feedback Control Systems for Unstable Plants with Saturating Actuators', *Proceedings IFAC Symposium - Nonlinear Control Systems Design*, Capri, 1989, pp. 302-307.

[19]Miotto P., Shewchun J.M., Feron E., and Paduano J.D., 'High Performance Bounded Control Synthesis with Application to the F18-HARV', *AIAA Guidance, Navigation, and Control Conference*, San Diego, CA, AIAA-96-3693, 1996.

[20]Belmont J.P., 'Mécanique du vol des avions aux grandes incidences', *Journée thématique DRET- La mécanique du vol des avions de combat, des missiles et des hélicoptères*, Paris, 1995.

[21]Doyle J.C., Packard A. and Zhou K., 'Review of LFTs, LMIs, and μ', *30th IEEE Conference on Decision and Control*, Brighton, 1991, pp. 1227-1232.

[22]Morton B.G., 'New Applications of μ to Real Parameter Variation Problems', *24th IEEE Conference on Decision and Control*, 1985, pp. 233-238.